Seismicity and seismic stress in the Coso Range, Coso geothermal field, and Indian Wells Valley region, southeast-central California

Joydeep Bhattacharyya
Joydeep Bhattacharyya Center for Monitoring Research, 1300 N. 17th Street, Suite 1450, Arlington, VA 22209, USA
Jonathan M. Lees
Department of Geology, University of North Carolina–Chapel Hill, Chapel Hill, North Carolina 27599, USA

ABSTRACT

The temporal and spatial distribution of seismicity in the Coso Range, the Coso geothermal field, and the Indian Wells Valley region of southeast-central California are discussed in this paper. An analysis of fault-related seismicity in the region led us to conclude that the Little Lake fault and the Airport Lake fault are the most significant seismogenic zones. The faulting pattern clearly demarcates the region as a transition between the San Andreas-type strike-slip regime to the west and the Basin and Range extension regime to the east. We present the spatial and temporal variations in seismicity immediately following significant earthquakes in nearby regions from 1983 to 1999 with special emphasis on larger earthquakes (M ≥ 5) in 1995–1998. The Ridgecrest earthquakes of 1995 show a complicated faulting pattern as the rupture changed from normal slip to right slip at depth. The interrelationships between the Coso Range earthquakes of 1996 and 1998 are presented as a set of conjugate events. Analysis of earthquake source mechanisms shows evidence for lateral variations in the faulting pattern in southeast-central California. Earthquake focal mechanisms are used to estimate local stress orientation within the Coso geothermal field. We have identified a boundary between a transpressional regime and a transtensional regime inside the field that correlates with observed spatial variations of heat flow and seismic attenuation, velocity, and anisotropy.

INTRODUCTION

The Coso Range, the Coso geothermal field, and the Indian Wells Valley region—one of the most seismically active regions of California—lies in southeast-central California. The region lies at the southwesternmost corner of the central Basin and Range geologic province of western United States (Fig. 1). The locations of the earthquakes, the spatial and temporal patterns of seismicity, and the earthquake source mechanisms are important tools for modeling the tectonics of this area. In this study, we use a large data set of earthquakes recorded between 1960 and 1999 to characterize the seismotectonics of the Coso Range, the Coso geothermal field, and the Indian Wells Valley. Tectonically, the Coso Range region is located at the transition from the extensional Basin and Range province to the strike-slip San Andreas fault system (Roquemore, 1980). North- to north-northeast–striking normal faults are dominant in the Coso Range (Duffield et al., 1980). Faulting is extensive in this region and includes two nearly perpendicular sets of normal faults that strike north-northeast and west-northwest (Roquemore, 1980).

The most seismically active region in our study area is the volcanic-geothermal field near Coso. The Coso geothermal field is situated in granitic Mesozoic basement rocks below silicic domes (Duffield and Bacon, 1981; Duffield et al., 1980). Pre-

Figure 1. Map of the Coso Range, Indian Wells Valley, and adjacent regions of southeast-central California. We show the topography of this region (in meters) along with the surface mapped faults (black lines), as given by Jennings (1994). The mountain ranges, valleys, and the towns of Darwin, Little Lake, and Ridgecrest are also indicated in this map.
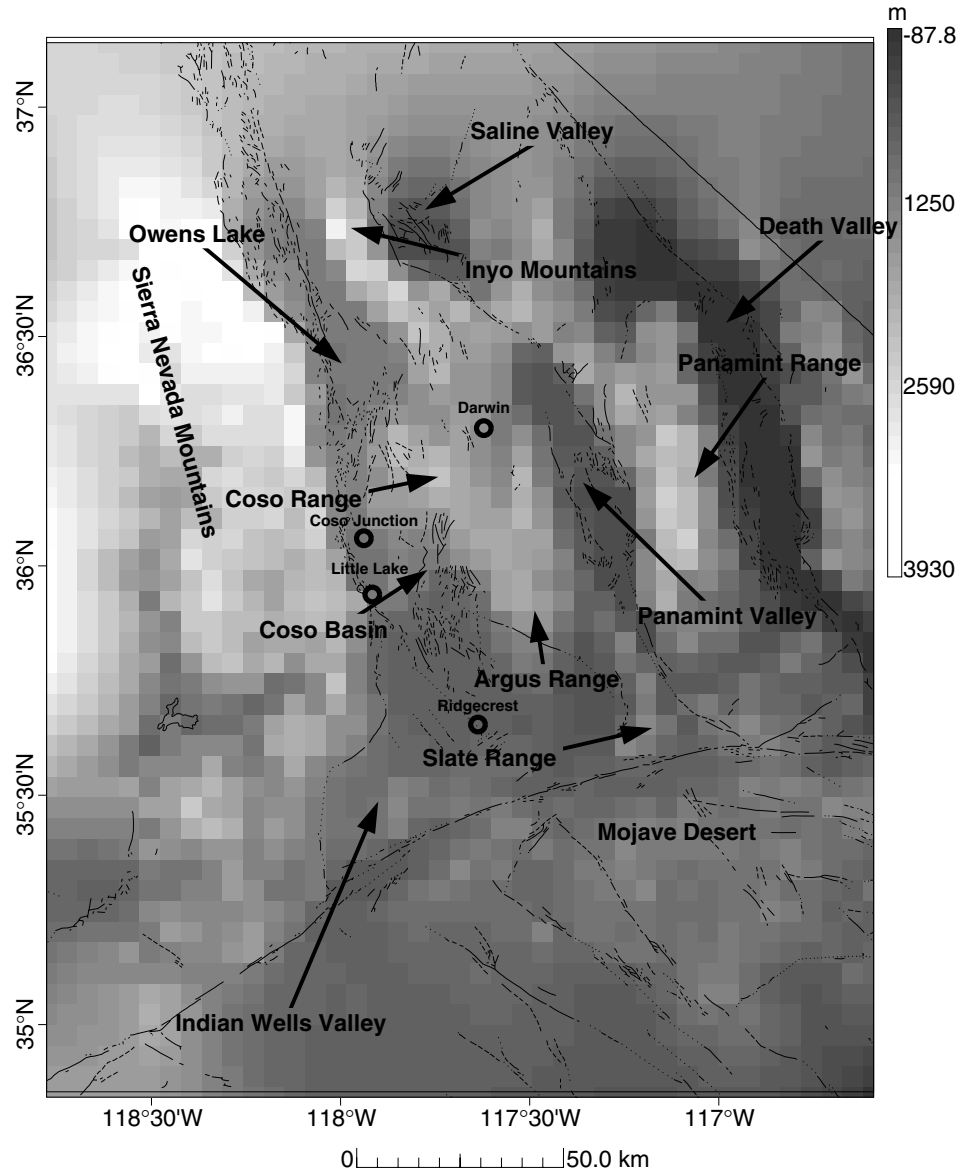
vious seismic studies of the Coso Range region using teleseismic traveltime residuals identified a low-velocity body in the mid-crust (below 5 km) southeast of the geothermal field (Reasenberg et al., 1980), which correlates with a high-attenuation anomaly (Sanders et al., 1988; Wu and Lees, 1996; Young and Ward, 1980). A silicic magma body, ~5 km in diameter and 1 km thick, probably partially molten, is predicted to lie at depths of >8 km under the Coso geothermal field (Bacon et al., 1980).

In this paper, we first identify the primary mapped faults in the study region and discuss the seismicity. We then describe the source mechanism and aftershock patterns of relatively large earthquakes that occurred in the region from 1995 to 1999. This description is followed by an analysis of spatial and temporal variations of present-day seismicity. Analysis of the source mechanisms of the earthquakes in this region allowed

us to map spatial variations of faulting pattern and also to investigate stress loading inside the Coso geothermal field due to large nearby earthquakes. The earthquake data sets used in the study were obtained from the microearthquake (MEQ) network located inside the Coso geothermal field (Alvarez, 1992), the Southern California Earthquake Center (SCEC), and the Northern California Earthquake Center (NCEC).

SEISMOTECTONIC SETTING

The seismotectonics of the Indian Wells Valley and the Coso Range primarily reflect the complex interaction of strike-slip faulting (San Andreas type) and extensional faulting (Basin and Range type). Fault-related seismicity is diminished inside the geothermal complex in the Coso volcanic field. Before an-

alyzing the seismicity within the Coso Range and the Indian Wells Valley, we first describe the nature and geometry of the significant faults in the region.

Indian Wells Valley

Tectonic and volcanic activity during the past 3 m.y. shaped much of the geomorphic and geologic character of the Indian Wells Valley. The region has been affected by several major faults such as the Garlock fault, the Sierra Nevada frontal fault system, and the Panamint Valley fault, which delineate the southern, western, and eastern boundaries of this region, respectively (Fig. 2). The Death Valley–Furnace Creek fault system is ~160 km east of this region. In addition to these faults, the Indian Wells Valley contains a number of north-striking
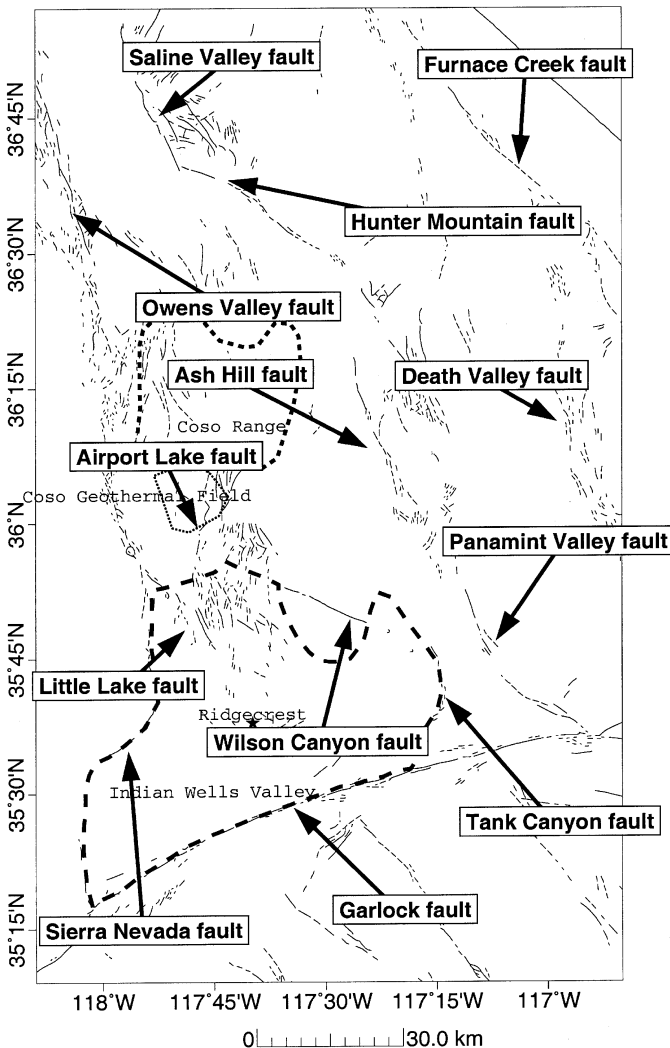

Figure 2. Fault map of the Coso Range, Indian Wells Valley, and adjacent regions (after Jennings, 1994). We have highlighted the significant faults of the region. The M = 8.0 Owens Valley earthquake was located at the intersection of the Little Lake fault and the Sierra Nevada fault.

faults (e.g., Little Lake fault, Airport Lake fault, Ash Hill fault); these consist of small fault segments mostly less than 10 km long (Fig. 2). The segments primarily trend north to northwest with a smaller number striking northeast. The faults merge in the north with the Sierra Nevada frontal fault near the rupture zone of the 1872 Owens Valley earthquake (Whitney, 1872). Southward, the segments form a broad zone of faulting truncated by the Garlock fault.

The Little Lake and the Airport Lake fault zones are the major active faults in the Indian Wells Valley (Fig. 2; Roquemore and Zellmer, 1983a). The Little Lake fault and Airport Lake fault were both formed by the regional tectonic stress field of the western Basin and Range province, i.e., right-slip shear and east-west extension. The pattern of faulting, though, differs between the Little Lake fault and the Airport Lake fault. The Little Lake fault shows predominantly right slip with a slight normal-slip component toward the central and the southern parts. On the other hand, the Airport Lake fault accommodates predominantly normal slip (Roquemore and Zellmer, 1983b).

The Little Lake fault strikes southeast from the Sierra Nevada fault diagonally across the Indian Wells Valley (Figs. 1 and 2) and is truncated at the Garlock fault. Slip rate along this fault is estimated at ~1.5 mm/yr (Roquemore, 1988; Simon McCluskey, 1988, personal communication). Near the intersection with the Sierra Nevada fault, the Little Lake fault has a dextral slip rate of ~0.6 mm/yr (Roquemore, 1981). Farther south along the Little Lake fault, the dominant motion becomes right-normal oblique. The right-slip component led Zellmer (1988) to suggest that the Little Lake fault may accommodate a major part of the right-slip motion of the Sierra Nevada fault in the Indian Wells Valley area.

The Airport Lake fault strikes north through the Indian Wells Valley and Coso Range. Southward, where the Airport Lake fault extends into the Indian Wells Valley, the fault zone consists of highly fragmented fault segments (Hart et al., 1989; Jennings, 1994). The Little Lake fault and the Airport Lake fault intersect in the Indian Wells Valley north of Ridgecrest (Fig. 2) in a zone characterized by high levels of seismicity and changes in the surface expression of the faults. This zone has been the focus of several studies (Hauksson et al., 1995; Roquemore and Zellmer, 1983b). Seismic tomographic studies of this zone by Sanders et al. (1988) indicated that it is underlain by a volume having very strong S-wave attenuation at a depth of ~3.0 km. Comparison with surface deformation and seismicity patterns suggests a recent intrusion of a dike (Roquemore, 1987). From a study of surface geologic features, Roquemore and Zellmer (1983a, 1983b) suggested that regional extension associated with the Airport Lake fault is transferred to the Little Lake fault as right-slip displacement within this zone of intersection.

Coso Range

The Coso Range lies at the transition between right-slip deformation across the San Andreas fault system and the

extensional regime of the Basin and Range. Recent folding and faulting show evidence of the characteristics of each of these provinces (Roquemore, 1980). Alternatively, the ring and arcuate faults in the Coso Range area have been explained in terms of caldera subsidence (Duffield, 1975). A recent study suggests that right-lateral shear is important to the fault structure of the Coso Range (Whitmarsh and Walker, 1996). Current strain accumulation in the Coso Range is modeled by north-striking right-lateral oblique-slip extensional faults (Roquemore et al., 1996). Present-day tectonic movements are expressed by widespread microearthquakes in the region (Walter and Weaver, 1980) though surface expressions of active faults are generally not observed (Roquemore and Simila, 1994).

Eastern California shear zone

The Coso Range, the Coso geothermal field, and the Indian Wells Valley lie within the Eastern California shear zone (Dokka and Travis, 1990a; Jones and Helmberger, 1998; Savage et al., 1990). The Eastern California shear zone extends ~500 km north-northwest from the San Andreas fault, through the Mojave Desert region, and beyond into Owens Valley and Death Valley. The Eastern California shear zone transfers a part of the relative motion between the North American and Pacific plates away from the San Andreas fault to the western Great Basin province (Dokka and Travis, 1990b). Individual faults within the region have slip rates of less than 1.0 mm/yr (Dokka, 1983). However, the total shear-displacement rate across the region from geologic and geodetic data is ~8.0 mm/yr (Dokka and Travis, 1990b; Savage et al., 1990). The Eastern California shear zone mainly consists of northwest-striking right-slip faults. The main earthquakes in the Eastern California shear zone include the 1992 M = 7.2 Landers earthquake and the 1872 M = 8.0 Owens Valley earthquake; they lie outside the region analyzed in this paper.

CHARACTERISTIC SEISMICITY

The Coso Range and Indian Wells Valley have a long history of earthquake swarms related to both tectonic and geothermal activity. Most of the earthquakes in the area are relatively small, i.e., M < 3.0. Large earthquakes (M > 4.9), although rare, have been recorded approximately every 20 years in this region until 1995—i.e., in 1938, 1961, 1982, and 1995 (Hauksson et al., 1995). The 1938 (M = 5.0; 9/17/38), 1961 (M = 5.2; 10/19/61), and 1982 sequences were on the Little Lake fault (Roquemore et al., 1996). The 1995 event occurred within the Airport Lake fault. This recurrence pattern may have been terminated by the occurrence of four M ≥ 5.0 earthquakes in this region between 1995 and 1998 (Bhattacharyya et al., 1999; Hauksson et al., 1995; Roquemore et al., 1996).

We divided the Coso Range–Indian Wells Valley region into several subregions (Fig. 3), for reasons described subsequently. The Coso Range is demarcated on the basis of the
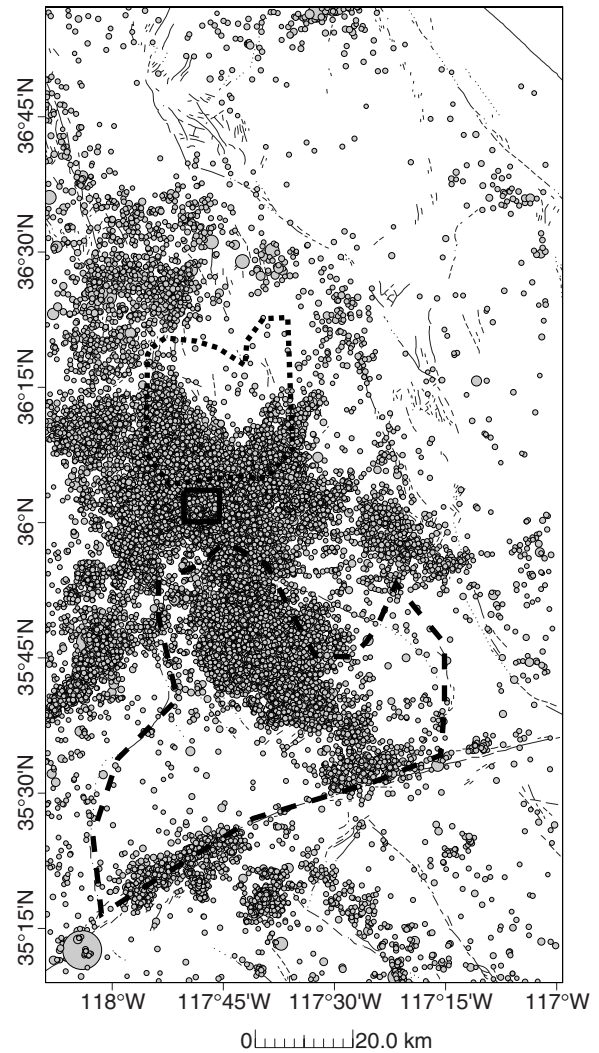

Figure 3. Seismicity in southeast-central California discussed in this paper. The seismicity of the Indian Wells Valley, the Coso Range, and the Coso geothermal field are separately discussed in the text. These regions are indicated by polygons, respectively. The faults given by Jennings (1994) are also shown.

definition of Duffield et al. (1980) except that we removed the geothermal field from the delineated area. Following Lees (2001), we defined the Coso geothermal field area as a box between lat 36.001°N and 36.059°N and between long 117.753°W and 117.834°W. The distinction between the Coso Range and the Coso geothermal field is made because of the difference in the earthquake sources that affect these regions. The seismicity in the Coso Range is due to rupture along mapped faults (Roquemore, 1987), but earthquakes in the Coso geothermal field are also due to the injection and production of geothermal fluids (Malin, 1994) and geothermal activity (Feng and Lees, 1998; Roquemore, 1987; Walter and Weaver, 1980). The boundaries of the Indian Wells Valley are based on those of Duffield et al. (1980).

Coso Range

Seismicity in the Coso Range (Fig. 3) primarily consists of microearthquakes (Combs, 1980; Feng and Lees, 1998; Malin, 1994). Prior to 1996, recorded earthquakes with magnitudes greater than 5.0 have occurred only on the periphery of the Coso Range. Among the largest of these earthquakes was the 1946 Walker Pass earthquake (M = 6.3). However, earthquake sequences with main-shock magnitudes greater than 5.0 occurred in the Coso Range in 1996 and 1998 (Bhattacharyya et al., 1999). We discuss these earthquakes subsequently in this paper.

Most of the earthquakes inside the Coso Range have been located toward the southern end of the region (Fig. 3). A detailed analysis of the spatial distribution of earthquakes indicates several sequences. From 1981 to 1984, most of the seismicity was concentrated toward the southwestern end of the Coso Range. The same region was reactivated in 1988 following the 10/13/88 M5.4 Nevada earthquake. In Figure 4, we plot the variation of seismicity and earthquake magnitudes with time. We show the cumulative distribution of earthquake size as given by $10M$ where M is the SCEC-provided magnitude of the earthquake (Fig. 4A). We use this measure as a rough estimate of seismic moment release. We observe that the monotonically increasing curve has several rapid increases ("jumps") immediately after the occurrence of large nearby earthquakes. In 1992, an increase of seismicity in the Coso Range was probably caused by seismic triggering due to the Landers event (6/28/92), which had a magnitude of M = 7.5 (Roquemore and Simila, 1994). Following the Eureka Valley earthquake of 5/27/93 (M = 6.1), there was a significant increase in seismicity in the Coso Range (Fig. 4). This seismicity was mostly located in the south-central part of the range (Fig. 3). The Coso Range earthquakes of 1996 and 1998 caused a distinct increase in seismicity in the region, as shown in Figure 4. The increased seismicity was mostly concentrated on the eastern side of the range. An interesting feature of the seismicity "jumps" is that the 1996 event caused a larger increase in seismicity, probably due to a larger source size. We observe a small increase in seismicity corresponding to the occurrence of the M = 6.4 Chalfant Valley earthquake on 7/21/86. The b-value (the slope of $\log(N)$ versus magnitude M, where N = number of earthquakes with magnitude M or less) of earthquakes within the Coso Range is 2.4.

Indian Wells Valley

There are very few large earthquakes in the Indian Wells Valley. Before 1995, the largest recorded earthquake to occur in the Indian Wells Valley itself was the M = 5.2 event in 1982 (Hauksson et al., 1995; Roquemore and Zellmer, 1983a). Prior to this event, several earthquake swarms were observed beginning during April 1981. Earthquakes with magnitudes between 4 and 5 initiated swarms (i.e., the swarms are possibly aftershocks) that lasted for more than 1 yr. The swarms were located along the intersection of the Little Lake and Airport Lake fault zones. With each successive sequence, the total number and maximum magnitude of earthquakes in each swarm increased as they migrated southward (Hauksson et al., 1995; Roquemore and Zellmer, 1983a). The 1982 event caused a large swarm in the central part of the valley.

Figure 5 shows the distribution of the magnitudes of the earthquakes in the Indian Wells Valley as a function of time. We observe that there are two "jumps" in seismicity in this region coinciding with significant regional events. The epicenters of the earthquake triggered by the Landers event trend north-northwest across the south-central part of the valley. Seismic activity following the Ridgecrest events was located close to the main-shock zone, which lies just north of the town of Ridgecrest. We do not see any evidence for increase in seismic activity in the Indian Wells Valley due to the Coso Range events of 1996 and 1998. The b-value for earthquakes within the Indian Wells Valley is 2.1 (Fig. 5C).

The Sierra Nevada fault marks the western edge of both the Coso Range and the Indian Wells Valley (Fig. 2). The southern end of the Sierra Nevada fault undergoes a bend between lat 35.25°N and lat 35.75°N; the seismicity drops drastically immediately south of this bend. From north to south, we observe a distinct increase in seismicity peaking in the region where the Sierra Nevada fault meets the Little Lake fault. In the northern part of the Sierra Nevada fault, we observe that seismicity is uniform with depth though a distinct decrease in seismicity can be seen in a 10-km-long region beginning just south of the town of Little Lake. The decrease in seismicity probably indicates a fundamental tectonic boundary south of the intersection of the Sierra Nevada fault with the Little Lake fault. The Little Lake fault is the most seismically active fault in the Indian Wells Valley region. Seismicity along this fault extends to 20 km depth. As seen in Figure 3, the intersection of the Little Lake fault and the Airport Lake fault is a region of intense seismicity, and relatively large earthquakes have been observed here (Hauksson et al., 1995). South of this region, i.e., between the junction of the Little Lake fault with the Airport Lake fault and the Garlock fault, we observe a noticeable drop in seismicity (Fig. 5). This drop in seismicity within a region that has a high seismicity rate may indicate a region of seismic quiescence and needs further analysis. Along the Airport Lake fault, seismicity is found to be uniform from the surface to a depth of 10 km.

The Coso geothermal field

Seismicity in the Coso geothermal field is controlled by the motion of geothermal fluids and the release of local tectonic stress (Feng and Lees, 1998; Fialko and Simons, 2000; Malin and Erskine, 1990; Walter and Weaver, 1980). The distribution and pattern of seismicity inside the field is described in detail in Feng and Lees (1998). We present the longer-term trends (1983–1999) in seismicity and the effect of nearby large earth-

Figure 4. Seismicity distribution and recurrence rate in the Coso Range. (A) Cumulative magnitude vs. time for 1983–1999. We calculate the magnitude as 10*kM*, where *M* is the magnitude of an earthquake as reported by SCEC. We use this measure as a proxy for moment release during each earthquake. The large earthquakes of the region, i.e., Rose Valley (2/19/92), Joshua Tree (4/22/92), Landers (6/28/92), Eureka Valley (5/27/93), M = 5.4 at Ridgecrest (8/17/95), M = 5.8 at Ridgecrest (9/20/95), Coso1 (11/27/96), and Coso2 (3/6/98), are indicated. We observe evidence for seismic triggering of the Landers, Eureka Valley, and the Coso1 earthquakes. (B) Distribution of earthquake magnitudes vs. time in the Coso Range. The increases in cumulative magnitudes in 1985 and 1988 are due to occurrence of M > 4.0 earthquakes in this region but cannot be associated with any significant (M ≥ 5) nearby earthquake. (C) Temporal distribution of earthquake magnitudes. We show the linear fit for the b-value calculation for this region. The b-value is calculated by using earthquakes with magnitudes ≥1.0 because the linear trend is not consistent below this magnitude, probably because of catalogue incompleteness at lower magnitudes. The b-value is slightly higher that what we observe at Indian Wells Valley.
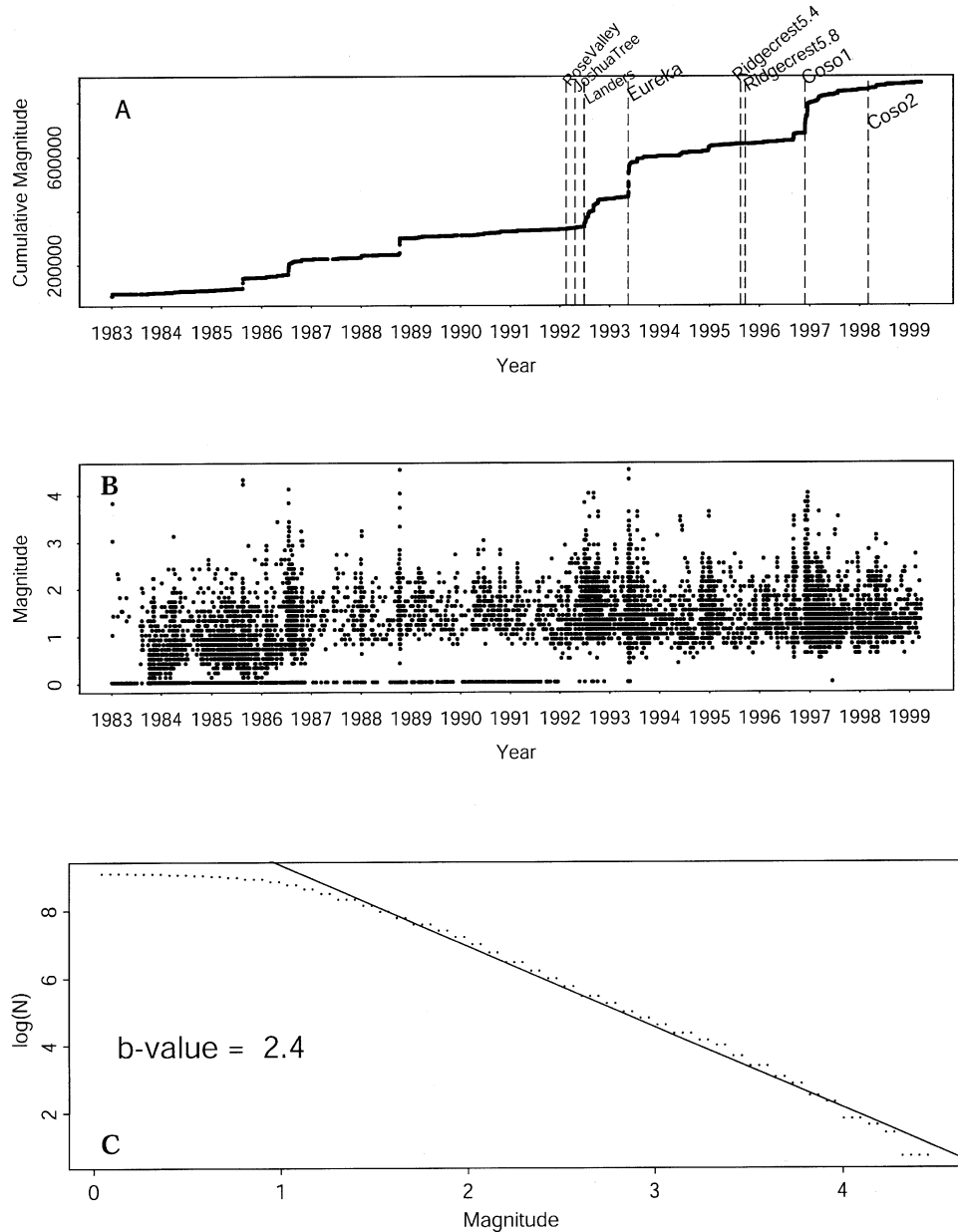
quakes. Seismicity inside the central geothermal area occurs in tight clusters inside a cylindrical region (Feng and Lees, 1998; Simila and Roquemore, 1987). Present-day daily average seismicity within the Coso geothermal field (Fig. 3) is ~22 events for earthquakes with the magnitude range M = −2.0 to 5.3 (as recorded by the MEQ network) (Bhattacharyya et al., 1999). Figure 6 shows the distribution of magnitude and cumulative magnitude inside the Coso geothermal field. In the cumulative distribution, the most prominent "jumps" follow the Ridgecrest events and the Coso Range events. We find that the increase in seismicity following the 1998 Coso Range earthquake is significantly larger than that following the 1996 Coso Range event. Main shocks for both of these events have nearly similar mag-

nitudes and lie approximately the same distance from the Coso geothermal field (Bhattacharyya et al., 1999). We suggest that the difference in associated seismicity is caused by the differences in source mechanism and thus in the stress-release pattern between the earthquakes. The smaller "jumps" in 1989 and 1999 are due to the occurrence of M = 3.0 events inside the geothermal field. It is interesting to note that an increase in cumulative seismicity in 1995 occurred before the Ridgecrest earthquakes.

Seismicity inside the Coso geothermal field shows several differences compared to that in the Coso Range and the Indian Wells Valley. Jumps in seismicity related to the occurrence of large regional events are much smaller in the Coso geothermal
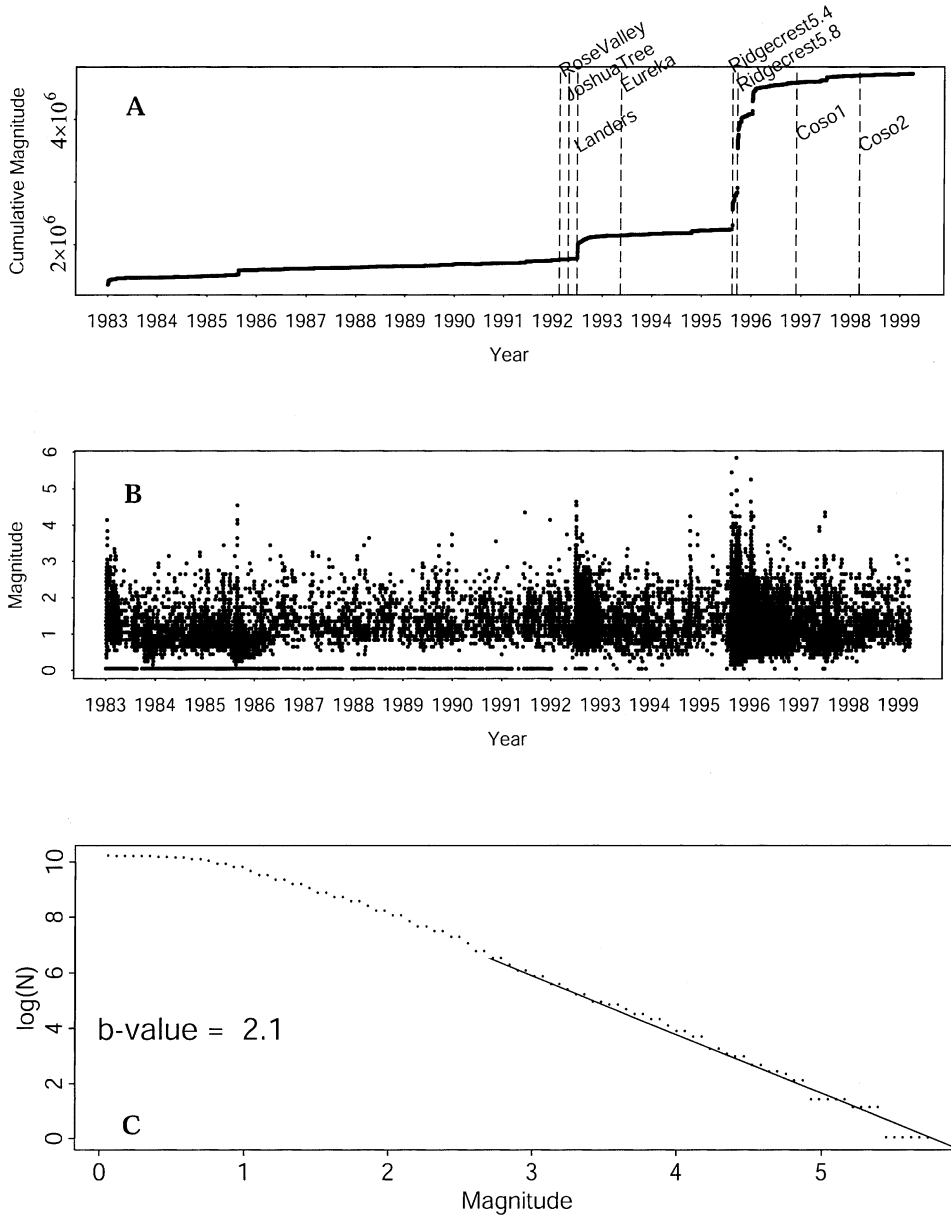
Figure 5. Seismicity distribution and recurrence rate in the Indian Wells Valley region. We observe a sharp increase in seismic moment release in the Indian Wells Valley following the Landers and the Ridgecrest events, indicating earthquake triggering following these earthquakes. The sharp increases in moment release in 1985, 1992, and 1995 are due to the occurrence of large earthquakes ($M \geq 4.0$).

field. The geothermal field generally is affected only by the nearby events, i.e., those near Ridgecrest and Coso, and not by the much larger, more distant, Landers earthquake. Lees (1998) found that the b-value in the field was not a constant function of magnitude. This result may be due to a physical effect in the geothermal field or a function of incompleteness of the catalogue; we cannot say for sure at this time. In the center of the distribution, where the catalogue is most reliable, the b-value was estimated to be 3.1, significantly higher than either the Indian Wells Valley or the Coso Range. Kisslinger and Jones (1991) and Creamer (1994) have shown that high temporal decay of earthquakes can be explained by high temperatures in seismogenic zones because rapid relaxation of residual stress due to heat flow is expected (Mogi, 1967). We postulate that

observed high b-values in the field are primarily due to the presence of geothermal fluids and much higher heat flow compared to the surrounding regions (Combs and Rotstein, 1976).

RECENT LARGE EARTHQUAKES IN THE COSO RANGE–INDIAN WELLS VALLEY REGION

Between 1996 and 1999, some of the largest earthquakes in California hit the Coso Range and the Indian Wells Valley, each with magnitudes $M \geq 5.0$. Although earthquakes in the Indian Wells Valley have similar source mechanisms (Hauksson et al., 1995), there is a fundamental change in the faulting for the Coso Range earthquakes, as described in this section (Bhattacharyya et al., 1999).
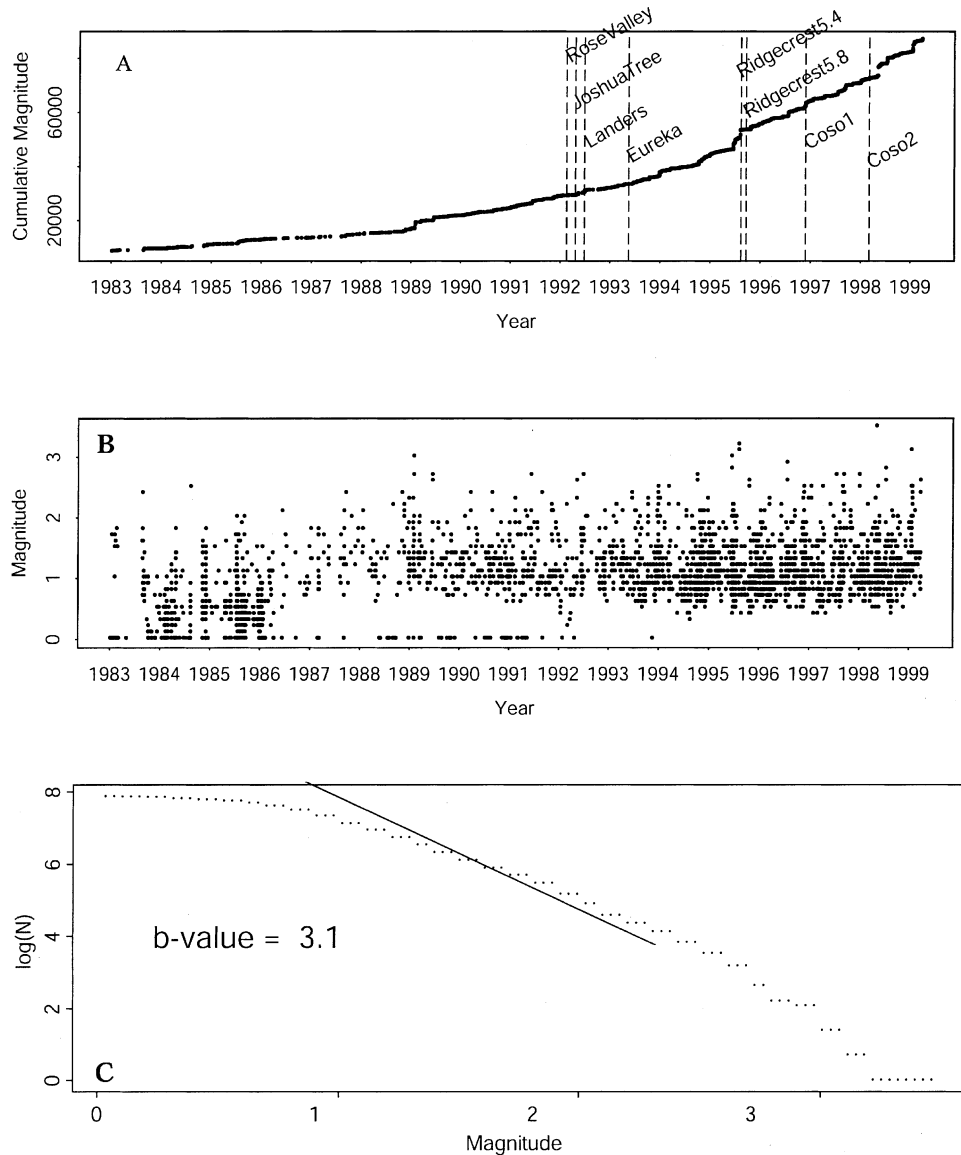
Figure 6. Seismicity distribution and recurrence rate inside the Coso geothermal field. Significant increases in seismic moment release occurred following the Ridgecrest and the Coso Range events. The small increase in 1989 coincides with the occurrence of relatively large earthquakes (M ∼ 3.0) inside the geothermal field. The temporal decay of earthquakes does not follow the linear pattern as expected by the Gutenberg-Richter theory, thereby giving b-values that vary with earthquake magnitude. We use the central (linear) part of the distribution (between M = 1 and M = 2.5) to obtain a b-value that is significantly higher than those obtained for the Coso Range or the Indian Wells Valley.

Ridgecrest earthquakes of 1995

In 1995, two large earthquakes occurred in the Indian Wells Valley near the town of Ridgecrest Fig. 7; (Hauksson et al., 1995). The first event (M = 5.4) occurred on August 17, 1995, along an active segment of the Airport Lake fault. This earthquake caused discontinuous surface cracking for ∼1 km along the fault and was centered 18 km north of the town of Ridgecrest (Roquemore et al., 1996). The M = 5.8 earthquake of September 20, 1995, possibly reruptured the same fault and had a maximum of 10 mm vertical and 8 mm right-slip displacement (Roquemore et al., 1996). This event was centered 2 km southeast of the August 17 earthquake. The aftershocks were located along three separate fault planes, and the focal mechanisms changed from normal slip to right slip at depth (Hauksson et al., 1995; Roquemore et al., 1996). The Ridgecrest earthquake of August 17 was followed by more than 2500 aftershocks over a period of five weeks, and 1900 aftershocks were recorded in the first two weeks following the September 20 event (Hauksson et al., 1995). The aftershocks migrated spatially; the seismic activity increased outward from the epicentral region in the northeast and southeast directions. The earthquake decay rates were consistent between both aftershock sequences with a b-value of ∼1.1.

The Coso Range earthquakes

Two recent earthquake sequences near the Coso geothermal field show clear evidence of faulting along conjugate planes (Fig. 7). Bhattacharyya et al. (1999) presented an analysis of aftershocks following the November 27, 1996, main shock and compared them to the March 6, 1998, event. The 1998 main
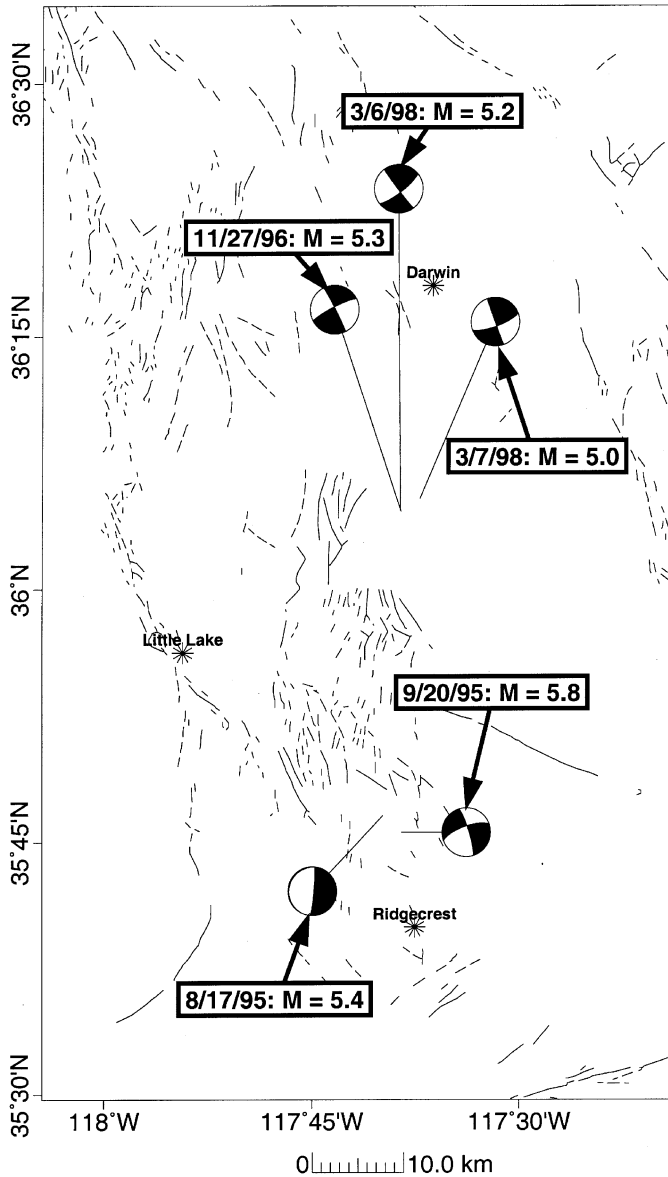
Figure 7. Large earthquakes near the towns of Coso Junction and Ridgecrest for 1995–1998. All of these earthquakes have a magnitude greater than 5.0. The source mechanisms were obtained from the SCEC.

shock ruptured with a local magnitude $M_L = 5.2$ and was located ~17 mi (~27 km) east-northeast of Little Lake, according to the SCEC. The main shock of the 1996 sequence had a local magnitude of 5.3. There were no observed surface ruptures associated with either of these earthquake sequences (Frank Monastero, 1998, personal communication). Although the 1998 and 1996 main shocks were located less than 900 m apart and had nearly the same M_L values, they differed significantly in their temporal and spatial behavior. The 1996 sequence b-value was 1.1, whereas that for the 1998 sequence was 0.85, a number close to the average southern California value. Moreover, the

1996 sequence was not followed by any significant (i.e., $M_L > 4.0$) aftershocks, but the 1998 sequence had four events of this magnitude.

A joint analysis of the fault-plane solutions of the main shocks and relocated aftershocks suggests that the two sequences ruptured along conjugate faults. Bhattacharyya et al. (1999) reported that, according to the conjugate-fault model, the 1996 main shock increased the shear stress acting across the fault that caused the 1998 events by ~0.15 MPa.

STRESS LOADING

The 1998 Coso Range earthquakes are used here to investigate stress loading in adjacent regions by using data from the three-component, short-period, high-dynamic-range borehole seismometers of the MEQ network.

Stress loading in the Coso geothermal field

To estimate the stress loading, we applied a stress step analysis defined as the change in static stress at the location of the earthquake produced by a different, nearby event (Bhattacharyya et al., 1999). The stress step is used to compute the change in failure stress in a region close to the main shock. The change in failure stress, a tensor field, is then compared to changes in seismicity, such that the change in aftershock locations is contrasted to the background seismicity. The MEQ data, where the recording seismic network remained the same before and after the main shock, give us a homogeneous recording that is especially suited for the stress analysis. We did not use events from other California catalogues because the MEQ stations are closer to the earthquakes (compared to, for instance, the stations of the Southern California Earthquake Network) and are therefore better for the detection, magnitude estimation, and location of microearthquakes required for a complete aftershock catalogue.

Bhattacharyya et al. (1999) estimated an average stress step of about $+100$ Pa inside the Coso geothermal field due to the $M > 4.5$ earthquakes of 1998, suggesting stress loading of the geothermal field. The Coso Range earthquakes were followed by a significant "jump" in seismicity inside the Coso geothermal field that was probably caused by this stress loading.

Results of stress loading

In this section, we describe three separate swarms inside the Coso geothermal field that occurred within a few months of the 1998 Coso Range main shock and probably were caused by the prestressing of the geothermal field. The main shocks for these sequences were events with $M \geq 3.0$. Injection and production of geothermal fluids has been continuous in the field for more than a decade. Although a significant number of earthquakes inside the field are due to geothermal-related activity, the recent events are the largest ones observed inside the Coso

geothermal field. Therefore, a connection between the nearby events and the earthquake swarms inside the field can be expected.

The largest event within the Coso geothermal field was the M = 3.5 earthquake of 5/10/98 (Fig. 8). The event was located at 2.1 km depth according to data recorded at the MEQ network. The aftershock sequence included nearly 200 earthquakes with magnitudes between $M_L = -2.6$ and 0.2. Preliminary analysis of the earthquake locations using P- and S-wave traveltimes clearly shows two distinct spatial populations. Earthquakes in one cluster align along an injection well, well 1, and are thought to be caused by fluid flow (Fig. 8). A second population forms a subhorizontal cluster that might be located along a structural feature such as a fault; however, it does not have any surface expression on geologic maps (e.g., Whitmarsh, 1998). Source mechanisms of the aftershocks do not show a clear spatial pattern although they may be complicated by the interaction of fluid overpressure with a subterranean zone of weakness.

Events in the second population propagated toward an adjacent production well, well 2, where the seismicity stops. This abrupt cessation of seismicity may be due to a release of overpressure at well 2. However, we do not have access to relevant well-log data (e.g., well-head pressure, lithology, etc.) that would allow us to explore this possibility. A subsequent swarm occurred in this region on July 16, 1998, giving rise to a series of earthquakes located along a potential weak zone, suggesting a reactivation of the same fault (Fig. 8). The second sequence was initiated by two earthquakes with M = 3.1 and 2.7, located at the junction of the fault and well 2. Compared to the first sequence, the number of aftershocks in this sequence is significantly fewer (= 17), and they have larger magnitudes ranging between M = −0.1 to 0.6.

The largest swarm of seismic activity inside the Coso geothermal field started on 12/29/98 (Fig. 9). This swarm was characterized by several relatively large (M ≥ 2.5) events and was initiated by an M = 3.4 main shock. Twelve more events, with
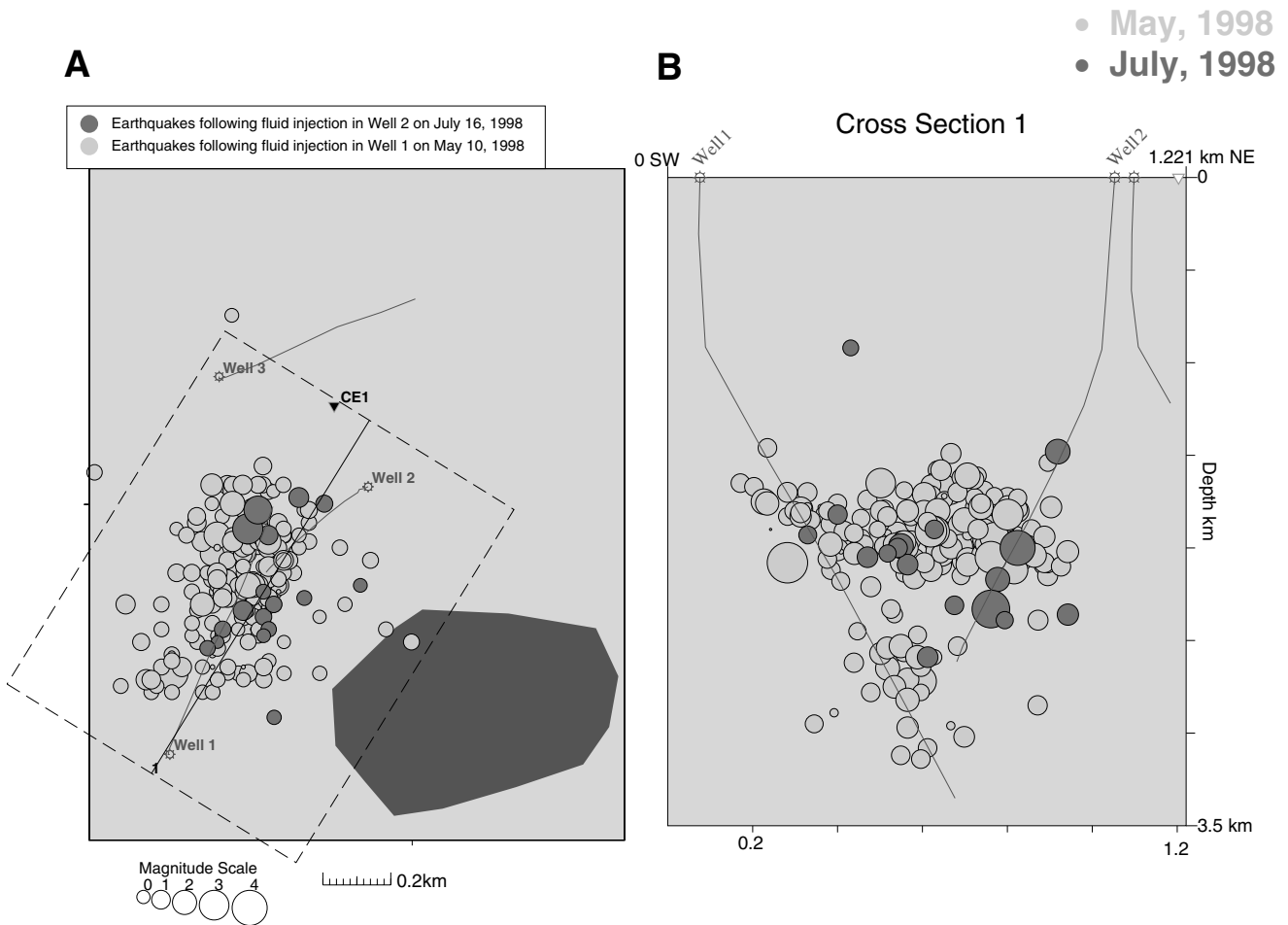

Figure 8. Locations of two earthquake swarms occurring inside the Coso geothermal field following a stress loading of the field due to the M = 5.2 event of 3/6/98; (A) map view and (B) cross section located along the solid line in A. We show the injection and production wells close to the swarms. Seismic station CE1 belongs to the MEQ network located inside the geothermal field. We can see that the seismicity lies along the wells and along a hypothesized subhorizontal fault at a depth of ~2.0 km.
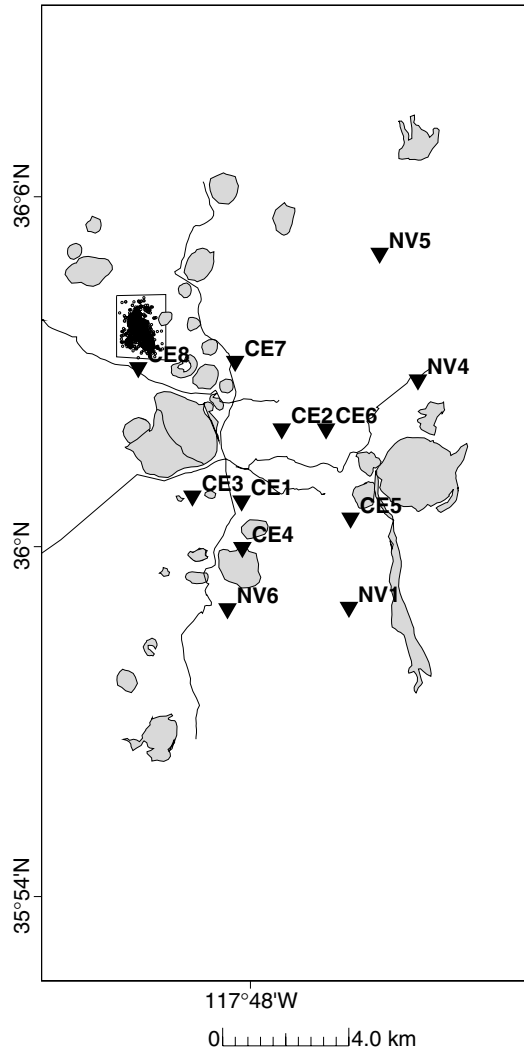
Figure 9. The earthquake swarm of December 1998–January 1999, located in the northwest corner of the Coso geothermal field. The rhyolite domes and the lava flows are indicated by the shaded regions. The locations of the seismic stations in the MEQ network are shown by CE and NV labels. The earthquakes in the swarm were located by using seismic waveforms recorded at the MEQ stations and a crustal model appropriate for the Coso geothermal field (Wu and Lees, 1999).

magnitudes $M \geq 2.5$, occurred during this sequence. The largest event of this swarm had a magnitude of 3.5. This region of the Coso geothermal field is the center of recent fumarolic activity, and the increased seismic activity may be due to increased movement of steam and geothermal fluids, although a quantitative analysis requires additional data (e.g., well logs, geodetic measurements, etc.).

ANALYSIS OF EARTHQUAKE SOURCE MECHANISM

The combination of source mechanisms and seismicity can be used to estimate the tectonic stress release of a region. A complete discussion of this topic should include geodetic mea-

surements and is therefore beyond the scope of this paper. We discuss two specific topics: (1) spatial distribution of earthquake source mechanisms and (2) orientation of principal stress axis inside the Coso geothermal field.

Distribution of earthquake source mechanisms

Focal mechanisms in the Coso Range–the Indian Wells Valley region are heterogeneously distributed, forming clusters of normal, strike-slip, normal-oblique-strike-slip, and oblique-normal fault styles. We have used focal mechanisms estimated by the program FPFIT (Reasenberg and Oppenheimer, 1985) applied to databases at SCEC and NCEC. Over 9000 events are shown in Figure 10. Because so many events are plotted on top of each other, we plot ternary diagrams (Frohlich, 1992) summarizing focal styles (Fig. 11). The ternary plots provide a means to quickly assess the spatial distribution of focal mechanisms when "beach-ball" plots are too congested. The entire target region is partitioned on a 10×10 grid, and all events within a block are summarized within a ternary plot. We reference the grid by designating the lower left-hand corner (1,1), and block numbers increase to the east and north. The overall sense of faulting in the Coso Range–Indian Wells Valley region ranges from normal to strike slip, in general agreement with Basin and Range extension and Pacific–North American plate boundary motion. Along the Garlock fault, strike-slip and oblique-normal patterns dominate (e.g., block 3,3). South of the Garlock fault, strike-slip mechanisms are most common (blocks 4,2 and 5,2). In the eastern part of the Ridgecrest event zone (blocks 4,6 and 4,7), normal and strike-slip faults are predominant, with virtually no reverse faulting evident. To the west (blocks 5,6 and 5,7), we see considerable reverse faulting for the earthquakes in this region. The Coso geothermal field is highlighted in Figure 11. Four blocks summarize the geothermal-field activity in this view. Note the increased presence of reverse faulting in the northwest corner of the geothermal field (block 3,9) as compared to the focal mechanisms in the other geothermal-field blocks (3,8; 4,8; and 4,9).

Stress orientation inside the Coso geothermal field

The geothermal field contains three major sets of faults thought to localize subsurface hydrothermal fluid circulation (Bishop and Bird, 1987; Roquemore, 1984). The first set consists of dextral strike-slip faults striking west-northwest that are well developed to the south and northwest of the Coso geothermal field (Fig. 1) (Duffield et al., 1980; Roquemore, 1984). The second set includes normal faults striking north to northeast and is well developed throughout the geothermal field. The third set comprises northeast sinistral strike-slip faults striking northeastward from the geothermal field (see Roquemore, 1984). The distribution of stress in the geothermal field was investigated by Feng and Lees (1998) who found a correlation in time and space of microseismicity with geothermal fluid
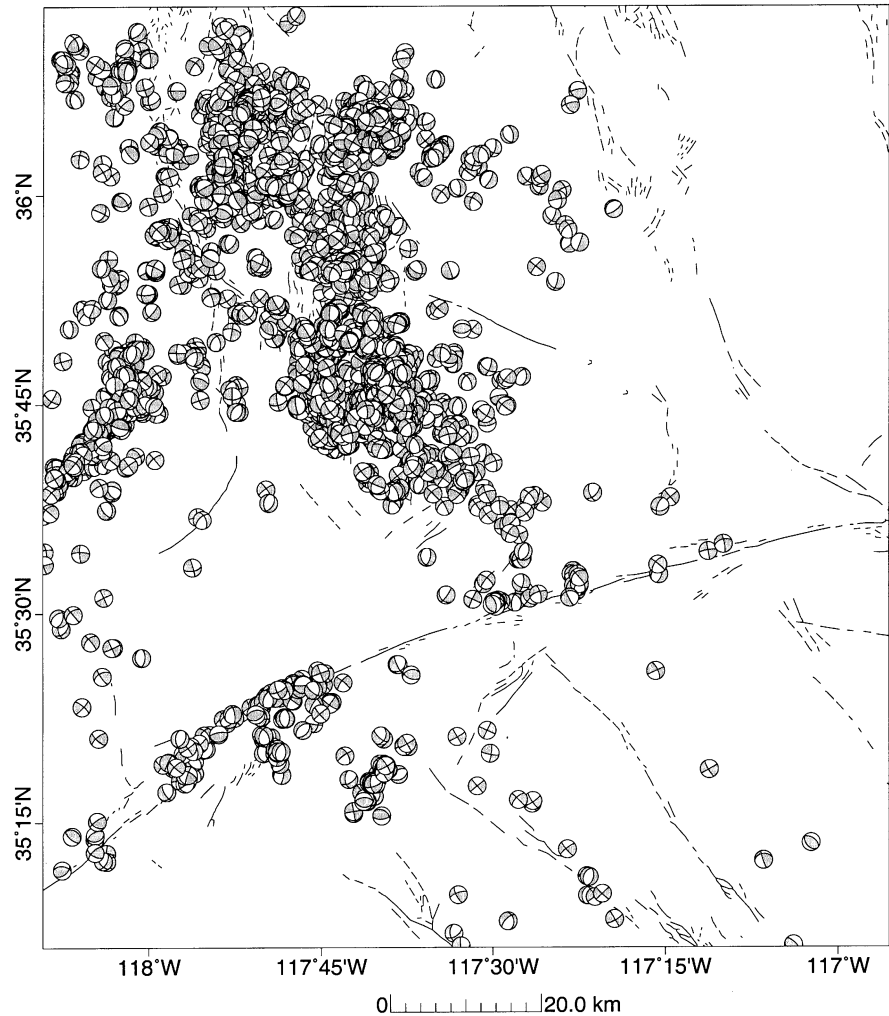
Figure 10. Focal mechanisms of earthquakes in the Coso Range and Indian Wells Valley of southeast-central California, obtained from SCEC.

injection and circulation at the Coso geothermal field. High-seismicity zones were found to indicate zones of high preexisting fracture density that may be the primary fluid-flow paths within the geothermal system. Stress patterns calculated from focal mechanisms showed a sharp transition from transpressional regimes in surrounding areas to transtensional regimes in the central area of the geothermal field. The stress transition defines the boundary between significantly different stress regimes within the field, primarily observed as a rotation of the maximum principal direction of stress. This boundary correlates with observed spatial variations of heat flow (Combs, 1980), seismic attenuation (Wu and Lees, 1996), P- and S-wave velocity (Wu and Lees, 1999), seismic anisotropy (Lees and Wu, 1999), and geochemical analyses. We conclude that stress regimes potentially represent separate blocks that differ geologically from north to south and are indicated by variations of stress orientation. Fialko and Simons (2000) interpreted the data to reflect contraction due to cooling.

SUMMARY

In this paper, we report on the spatial and temporal distribution and source mechanisms of earthquakes occurring in the Coso Range–Indian Wells Valley region. We identify zones of significant seismic activity, investigate their relationship to mapped faults, and quantify the lateral variation of stress changes and faulting patterns. The important structural controls for this region are as follows:

1. The Coso Range–Indian Wells Valley region, which belongs in the Eastern California shear zone, marks a transition between the strike-slip tectonics of San Andreas fault and the extensional tectonics of the Basin and Range province. The regional deformation direction is north-northwest–trending right-lateral shear.

2. The Little Lake fault and the Airport Lake fault are the most significant active faults in the Indian Wells Valley. Several inactive faults are also present. Seismicity in the Coso Range area is mostly located in the Coso geothermal field.
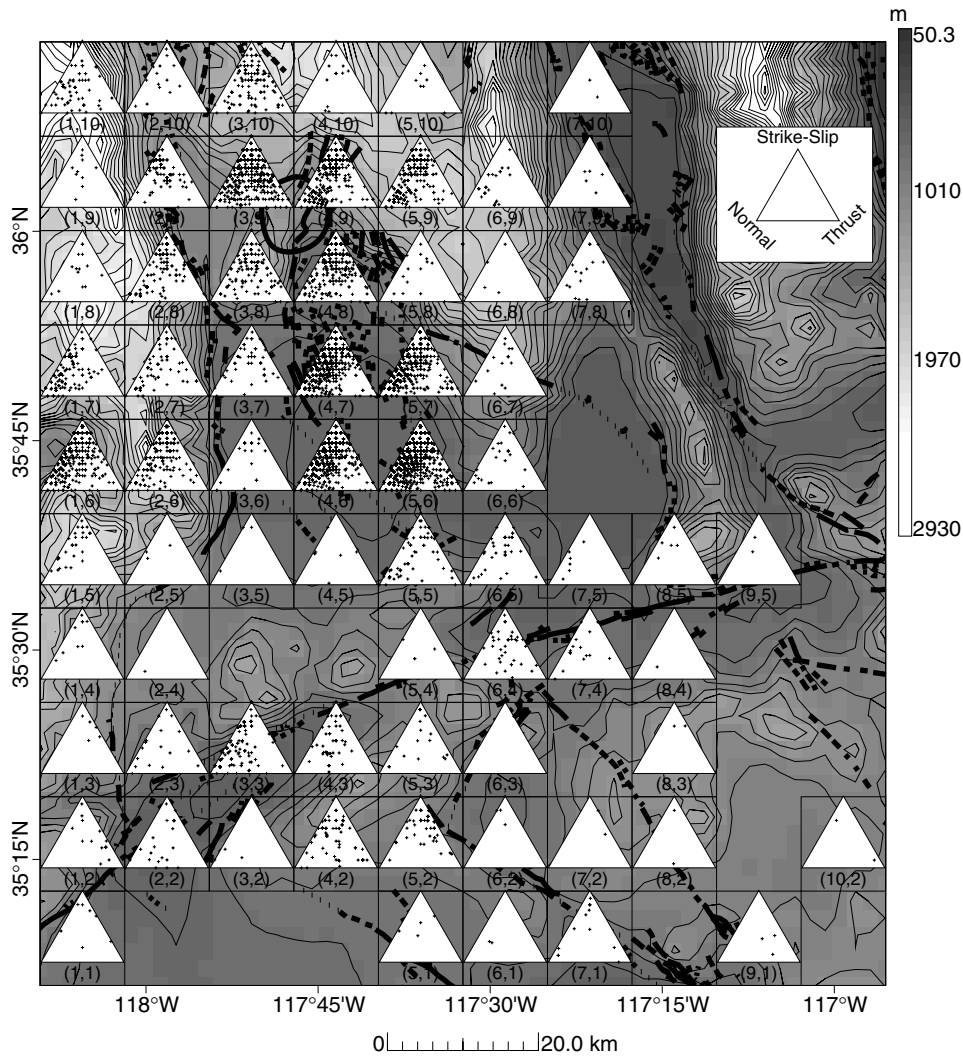
Figure 11. Ternary diagrams (Frohlich, 1992) for southeast-central California summarizing focal styles in different subregions. In each ternary diagram, strike-slip faults are plotted at the top apex, normal faults on the bottom left, and thrust faults on the bottom right. For reference, topographic relief is contoured and an outline of the Coso geothermal field is shown by a bold circle at 36°N, 117°47′W.

3. Seismicity in the Indian Wells Valley is mostly characterized by swarms of earthquakes. Earthquakes in the Coso Range area are related to tectonic motion and geothermal activity.

4. We observe significant increase in seismicity in the Indian Wells Valley due to the 1992 Landers event and the 1995 Ridgecrest earthquakes. The increase in seismicity is much smaller in the geothermal field, possibly because of the elevated temperatures in the seismogenic zone.

5. The faults of the Coso Range–Indian Wells Valley region generally accommodate normal to strike slip, reflecting the transition between extensional and strike-slip tectonics. Lateral variations of source mechanisms were used to map stress changes inside the Coso geothermal field. The central geothermal area belongs to a transtensional regime and is surrounded by a region under transpression.

6. The Coso Range earthquake of 1998 caused stress loading inside the geothermal field. Some of the largest earthquakes inside the geothermal field occurred within months of this event, although the events cannot be clearly related without further corroborative data, e.g., well logs.

ACKNOWLEDGMENTS

REFERENCES CITED

Alvarez, M.G., 1992, The seismotectonics of the southern Coso Range observed with a new borehole seismograph network [M.S. thesis]: Duke University.

Bacon, C.R., Duffield, W.A., and Nakamura, K., 1980, Distribution of quaternary rhyolite domes of the Coso range, California: Implications for extent of the geothermal anomaly: Journal of Geophysical Research, v. 85, p. 2425–2433.

Bhattacharyya, J., Grosse, S., Lees, J.M., and Hasting, M., 1999, Recent earthquake sequences at Coso: Evidence for conjugate faulting and stress loading near a geothermal field: Bulletin of the Seismological Society of America, v. 89, p. 785–795.

Bishop, B.P., and Bird, D.K., 1987, Variation in sericite compositions from fracture zones within the Coso hot springs geothermal system: Geochemica et Cosmochemica Acta, v. 51, p. 1245–1256.

Combs, J., 1980, Heat flow in the Coso geothermal area, Inyo County, California: Journal of Geophysical Research, v. 85, p. 2411–2424.

Combs, J., and Rotstein, Y., 1976, Microearthquake studies at the Coso Geothermal Area, China Lake, California [abs,]: Proceedings of the 2nd United Nations Symposium on the Development and Use of Geothermal Resources, p. 909–916.

Creamer, F.H., 1994, The relation between temperature and earthquake aftershock decay for aftershock sequences near Japan [Ph.D. thesis]: University of Colorado.

Dokka, R.K., 1983, Displacements on late Cenozoic strike-slip faults of the central Mojave Desert, California: Geology, v. 11, p. 305–308.

Dokka, R.K., and Travis, C.J., 1990a, The eastern California shear zone and its role in the tectonic evolution of the Pacific-North American transform boundary: Geological Society of America Abstracts with Programs, v. 22, no. 3, p. 19.

Dokka, R.K., and Travis, C.J., 1990b, Role of the eastern California shear zone in accommodating Pacific-North American plate motion: Geophysical Research Letters, v. 17, p. 1323–1326.

Duffield, W.A., 1975, Late Cenozoic ring faulting and volcanism in the Coso Range area of California: Geology, v. 3, p. 335–338.

Duffield, W.A., and Bacon, C.R., 1981, Geologic map of the Coso volcanic field and adjacent areas, Inyo County, California: US Geological Survey Map, scale 1:62 500.

Duffield, W.A., Bacon, C.R., and Dalrymple, G.B., 1980, Late Cenozoic volcanism, geochronolgy, and structure of the Coso Range, Inyo County, California: Journal of Geophysical Research, v. 85, p. 2381–2404.

Feng, Q., and Lees, J.M., 1998, Microseismicity, stress, and fracture within the Coso geothermal Field, California: Tectonophysics, v. 289, p. 221–238.

Fialko, Y.A., and Simons, M., 2000, Deformation and seismicity in the Coso geothermal area, Inyo County, California: Observations and modeling using satellite radar interferometry: Journal of Geophysical Research, v. 105, p. 21 781–21 794.

Frohlich, C., 1992, Triangle diagrams: ternary graphs to display similarity and diversity of earthquake focal mechanisms: Physics of the Earth and Planetary Interiors, v. 75, p. 193–198.

Hart, E.W., Bryant, W.A., Wills, C.J., Treiman, J.A., Kahle, J.E., 1989, Fault evaluation program, 1987–1988, southwestern Basin and Range region and supplemental areas: Open File Report 89-16, California Division of Mines and Geology, p. 31.

Hauksson, E., Hutton, K., Kanamori, H., Jones, L., Mori, J., Hough, S., and Roquemore, G., 1995, Preliminary report on the 1995 Ridgecrest earthquake sequence in eastern California: Seismological Research Letters, v. 66, p. 54–60.

Jennings, C.W., 1994, Fault activity map of California and adjacent areas with location and ages of recent volcanic eruptions: California Division of Mines and Geology, California Geologic Data Map Series, Map No. 6.

Jones, L.E., and Helmberger, D.V., 1998, Earthquake source parameters and fault kinematics in the Eastern California Shear Zone: Bulletin of the Seismological Society of America, v. 88, p. 1337–1352.

Kisslinger, C., and Jones, L.M., 1991, Properties of aftershock sequences in southern California: Journal of Geophysical Research, v. 96, p. 11947–11958.

Lees, J.M., 1998, Multiplet analysis at Coso Geothermal: Bulletin of the Seismological Society of America, v. 88, p. 1127–1143.

Lees, J.M., and Wu, H., 1999, P-wave anisotropy, stress, and crack distribution at Coso Geothermal Field, California: Journal of Geophysical Research, v. 104, p. 17955–17973.

Malin, P., 1994, The seismology of extensional hydrothermal system: Geothermal Resources Council, v. 18, p. 17–22.

Malin, P.E., and Erskine, M.C., 1990, Coincident P and SH reflections from basement rocks at Coso geothermal field: American Association of Petroleum Geologists Bulletin, v. 74, p. 711.

Mogi, K., 1967, Earthquakes and fractures: Tectonophysics, v. 5, p. 35–55.

Reasenberg, P., Ellsworth, W., and Walter, A., 1980, Teleseismic evidence for a low-velocity body under the Coso Geothermal Area: Journal of Geophysical Research, v. 85, p. 2471–2483.

Reasenberg, P., and Oppenheimer, D.H., 1985, FPFIT, FPPLOT and FPPAGE: Fortran computer programs for calculating and displaying earthquake fault-plane solutions.

Reasenberg, P., and Oppenheimer, D.H., 1985, FPFIT, FPPLOT and FPPAGE; Fortran computer programs for calculating and displaying earthquake fault-plane solutions: U.S. Geological Survey Open File Report 109.

Roquemore, G., 1980, Structure, tectonics, and stress field of the Coso Range, Inyo County, California: Journal of Geophysical Research, v. 85, p. 2434–2440.

Roquemore, G., 1988, Revised estimates of slip-rate on the Little Lake Fault, California: Geological Society of America Abstracts with Programs, v. 20, no. 3, p. 225.

Roquemore, G., Simila, G.W., and Mori, J., 1996, The 1995 Ridgecrest earthquake sequence: new clues to the neotectonic development of the Indian Wells Valley and the Cos Range, eastern California: Geological Society of America Abstracts with Programs, v. 28, no. 5, p. 106.

Roquemore, G., and Zellmer, J., 1983a, Ground cracking associated with the 1982 Magnitude 5.2 Indian Wells Valley earthquake: California Geology, v. 36, p. 197–200.

Roquemore, G., and Zellmer, J., 1983b, Tectonics, Seismicity, and volcanism at the Naval Weapons Center: Naval Research Reviews, v. 35, p. 3–9.

Roquemore, G.R., 1981, A hypothesis to explain anomalous structures in the western Basin and Range Province: US Geological Survey Open File Report, 81-0503.

Roquemore, G.R., 1984, Ground magnetic survey in the Coso Range, California: Journal of Geophysical Research, v. 89, p. 3309–3314.

Roquemore, G.R., 1987, The microseismicity of the shallow geothermal reservoir in the Coso Range, California: Seismological Research Letters, v. 58, p. 29.

Roquemore, G.R., and Simila, G.W., 1994, Aftershocks from the 28 June 1992 Landers earthquake, northern Mojave Desert to the Coso volcanic field, California: Bulletin of the Seismological Society of America, v. 84, p. 854–862.

Sanders, C., Ho, L.P., Rinn, D., and Kanamori, H., 1988, Anomalous shear wave attenuation in the shallow crust beneath the Coso volcanic region, California: Journal of Geophyical Research, v. 93, p. 3321–3338.

Savage, J.C., Lisowski, M., and Prescott, W.H., 1990, An apparent shear zone trending north-northwest across the Mojave Desert into Owens Valley, eastern California: Geophysical Research Letters, v. 17, p. 2113–2116.

Simila, G.W., and Roquemore, G.R., 1987, Earthquake history of the Owens Valley region, in Gath, E.M., Gregory, J.L., Sheehan, J.R., Baldwin, E.J., and Hardy, J.K., eds., Geology and mineral wealth of the Owens Valley region, California: Annual Field Trip Guidebook, South Coast Geological Society, p. 145–156.

Walter, A.W., and Weaver, C.S., 1980, Seismicity of the Coso Range, California: Journal of Geophysical Research, v. 85, p. 2441–2458.

Whitmarsh, R., 1998, Structural development of the Coso Range and adjacent areas of eastern California [Ph.D. thesis]: University of Kansas.

Whitmarsh, R.W., and Walker, J.D., W.?????, 1996, Structural domains within the Coso Range of east-central California: a case for right-oblique extension: Geological Society of America Abstracts with Programs, v. 28, no. 7, p. 116.

Whitney, J.D., 1872, The Owens Valley earthquake: Overland Monthly, p. 130–140.

Wu, H., and Lees, J.M., 1996, Attenuation structure of the Coso Geothermal area, California, from pulse width data of P-wave: Bulletin of the Seismological Society of America, v. 86, p. 1574–1590.

Wu, H., and Lees, J.M., 1999, Three-dimensional *P* and *S* wave velocity structures of the Coso Geothermal Area, California, from microseismic traveltime data: Journal of Geophysical Research, v. 104, p. 13 217–13 233.

Young, C.Y., and Ward, R. W., 1980, Three-dimensional Q^{-1} model of the Coso Hot Springs known geothermal resource area: Journal of Geophysical Research, v. 85, p. 2459–2470.

Zellmer, J.T., 1988, Engineering and environmental geology of the Indian Wells Valley area, southeastern California: Association of Engineering Geologists, v. 25, p. 437–457.